PCCP

Accepted Manuscript

ROYAL SOCIETY OF CHEMISTRY

www.rsc.org/pccp

Aggregation induced blue-shifted emission – molecular picture from QM/MM study†

Qunyan Wu,‡[a] Tian Zhang,‡[a] Qian Peng,*[b] Dong Wang,[a] and Zhigang Shuai*[a]

[a]Key Laboratory of Organic OptoElectronics and Molecular Engineering, Department of Chemistry, Tsinghua University, Beijing 100084, P. R. China. Email: zgshuai@tsinghua.edu.cn

[b]Key Laboratory of Organic Solids, Beijing National Laboratory for Molecular Science (BNLMS), Institute of Chemistry, Chinese Academy of Sciences, Beijing 100190, P. R. China. Email: qpeng@iccas.ac.cn,

†Electronic supplementary information (ESI) available: supplementary figures and tables. See DOI: 10.1039/b000000x

‡These authors contributed equally.

ABSTRACT

In general, optical emission in solid-state is red-shifted with respect to solution phase. A series of recently synthesized compounds exhibits aggregation induced blue-shifted emission (AIBSE) phenomena. By employing a polarizable continuum model (PCM) and a hybrid quantum mechanics/molecular mechanics (QM/MM) approach, we investigate the excited-state electronic structures for some typical AIE-active molecules both in solvents and in aggregates at the time-dependent density functional theory (TD-DFT) level. It is found that the AIBSE phenomena is originated from the smaller reorganization energy in aggregate than the solution phase, as evidenced through the restricted structural relaxation, planarization in the excited state, and freezing of low-frequency out-of-plane twists in the state transition.

KEYWORDS

Aggregation induced blue-shifted emission (AIBSE), PCM, QM/MM

1. Introduction

Efficient luminescent materials have attracted great attention due to their potential applications in solid-state display and lighting devices and bio-sensing. Most organic optoelectronic devices operate in solid state.[1-4] It has been long known that molecular aggregate often causes both luminescence quenching and emission red-shift. There are several origins for the former: (i) intermolecular charge transfer which reduces the probability for electron-hole recombination; (ii) intermolecular excitation energy transfer eventually to trap state; (iii) or formation of the low emissive 'side-by-side' H-aggregates with dipole-forbidden nature of the emitting state[5] or detrimental species such as excimers with strong π-π interactions.[6-7] Gierschner *et al.* demonstrated recently that for a class single crystals with H-aggregate packing can be highly emissive, in sharp contrast to the conventional wisdom [8]. The aggregation-induced red-shifted emission spectra could be ascribed to (i) excitonic coupling resulting from Coulombic interaction of spatial distribution of the transition dipole densities;[8] (ii) the anisotropic polarizability induced by the crystalline envirionment;[9-10] (iii) the charge-transfer (CT) character giving rise to a new intermolecular coordinate in the geometry change in π-stacks;[5] (iv) formation of J-aggregates;[5,11] (v) the smaller band gap rising from the increased band widths of both the HOMO- and the LUMO- derived band according to a tight-binding model.[12] Thus, it is intriguing for compounds exhibiting aggregation induced blue-shifted emission (AIBSE) phenomena. The blue-shifted solid-state emission spectra were early observed in the substituted oligophenylenevinylenes (**OPV**) microcrystals.[9,13]

Then, it is found to be widely present in the solid-phase strong emitters with the so-called "aggregation-induced emission" (AIE) characteristic.[6,14-20] For example, the absorption band of 9,10-distyrylanthracene (**DSA**) in dilute THF solution peaks at 407 nm (3.05 eV), and the photoluminescence spectrum exhibits orange emission with a peak at 612 nm (2.03 eV).[15] While the absorption band for solid **DSA** particles in THF/H_2O mixture (THF/H_2O = 1:3 v/v) is very similar to that in dilute THF solution, peaking at 414 nm (2.99 eV),[14] but the emission spectrum of **DSA** crystal exhibits obvious blue-shifted peak at 518 nm (2.39 eV).[15] The absorption and emission maxima of 2,3-dicyano-5,6-diphenylpyrazine (**DCDPP**) in dilute THF solution are 340 nm (3.65 eV) and 423 nm (2.93 eV), respectively.[16] When mixing 90% volume fraction of water in THF, the absorption peak of **DCDPP** suspension in THF/H_2O mixture keeps unchanged, but the emission spectrum shows a blue-shifted peak at 413 nm (3.00 eV).[16] The absorption and emission maxima of *cis*,*cis*-1,2,3,4-tetraphenyl-1,3-butadiene **(TPBD)** in dilute acetone solution are 334 nm (3.71 eV) and 408 nm (3.04 eV), respectively.[17] When adding 90% volume fraction of water to acetone, the absorption peak of **TPBD** aggregates in acetone/H_2O mixture experiences a slight red shift peaking at 344 nm (3.60 eV), but the emission spectrum shows a blue-shifted peak at 390 nm (3.18 eV).[17]

The AIBSE phenomena are quite surprising experimental findings and the underlying mechanism is still unclear due to the difficulty in microscopic structural characterization. It was speculated that the twisted conformation in the solid state leads to less effective delocalization, which might be responsible for the blue shifts.[6,

[14] However, this would cause both blue-shifted absorption and emission. Another speculation is the formation of twisted intramolecular charge transfer (TICT) state in the polar solvent and locally excited state in aggregate due to restricted intramolecular rotation, which causes intensified and blue-shifted emission in the solid state.[21] However, this requires the molecule to contain strong donor and acceptor groups. In fact, the experimental observation shows that there is a slight red shift or hardly any shift in absorption, while the emission is remarkably blue-shifted. **DSA**, for example, when going from dilute tetrahydrofuran (THF) solution to solid state, its absorption maximum undergoes a slight red shift (7 nm, 0.06 eV), but its emission maximum experiences a quite remarkable blue shift (94 nm, 0.36 eV) from 612 nm to 518 nm, with an approximately 100-fold increment in its fluorescence quantum yield.[14-15]

To better understand the mechanisms of such intriguing AIBSE phenomena, we have carried out theoretical and computational investigations for the excited-state structures both in dilute solution and in aggregate. Previously, the AIE phenomena have been theoretically explored by performing quantum mechanical/molecular mechanical (QM/MM) calculations, which provided a quantitative understanding.[22-24] In this contribution, we adopted the same computational approach to mimic the aggregation behaviors of **DSA**, **DCDPP**, and **TPBD** (**Chart 1**). Through carefully analyzing geometric and excited-state energetic properties of these molecules both in dilute solution and aggregate, we found that the blue-shifted emission is originated from the smaller reorganization energy in aggregate compared to the solution phase,

which is induced by restricted geometric relaxation from $\mathbf{S_1}$ to $\mathbf{S_0}$, excited-state planarization and freezing of low-frequency out-of-plane vibrations.

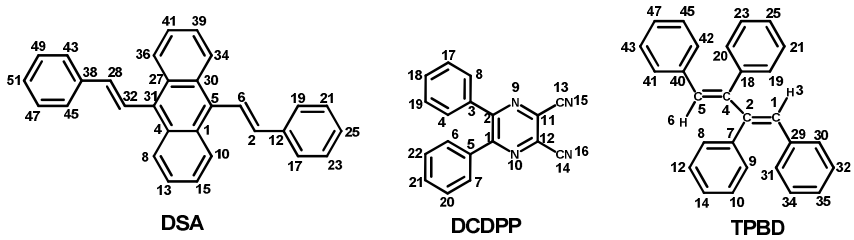

Chart 1. The chemical structures of **DSA**, **DCDPP**, and **TPBD**.

2. Theoretical model and Computational Methodology

The basic model adopted in this work is the adiabatic potential-energy surface (PES) as shown in **Chart 2**, and Q refers to the nuclear configuration. $E_{\mathrm{em(ab)}}$ is the emission (absorption) energy, and $\lambda_{\mathrm{gs(es)}}$ is the reorganization energy of the ground state $\mathbf{S_0}$ (the first excited state $\mathbf{S_1}$). The total reorganization energy (λ), which corresponds to the Stokes shift observed in experiment, is expressed as the sum of λ_{gs} and λ_{es}. The emission energy can be expressed as the absorption energy minus the total reorganization energy:

$$E_{\mathrm{em}} = E_{\mathrm{ab}} - \lambda \tag{1}$$

When going from aggregate (*aggr*) to solution (*sol*), the shifted emission is obtained through simple subtraction:

$$\Delta E_{\mathrm{em}}^{aggr-sol} = \Delta E_{\mathrm{ab}}^{aggr-sol} + \lambda^{sol-aggr} \tag{2}$$

We note that for strongly coupled excitons or excimer-like π-π interaction, in both absorption and emission, there should be $\Delta E^{aggr-sol} < 0$, namely, the normal red shift.

However, for some AIE-active molecules, usually with several twistable phenyl rings attached to the conjugated backbone of the chromophores, the intermolecular π-π stacking is often negligible due to large intermolecular π-π interaction distance in crystals (Fig. S1-S3†), and the intramolecular motions dominate the photophysical processes.[22-24] In this case, the λ term could be much more pronounced in solution than that in aggregate, resulting in a large positive term $\lambda^{sol-aggr}$ in Equation (2). Thus, the emission can exhibit a remarkable blue shift if the absorption shift is minor, whether red or blue. The blue-shifted emission implies $\Delta E_{\mathrm{em}}^{aggr-sol} > 0$.

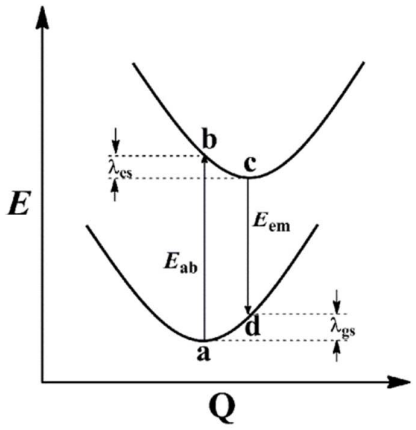

Chart 2. Schematic representation of the adiabatic potential energy surfaces (PES) for $\mathbf{S_0}$ and $\mathbf{S_1}$.

We build our computational models as illustrated in **Chart 3**. We look at the molecular structures at both the ground state and the first excited state, in solution phase and in aggregate phase, respectively. The solvent effect is modeled using polarizable continuum model (PCM).[25-27] The aggregate is modeled by an approach combining quantum mechanics and molecular mechanics (QM/MM),[28] where one

electronically excited molecule is treated by the time-dependent density functional theory (TD-DFT), and the surrounding molecules are modeled with the general Amber force field (GAFF).[29] The aggregate structure is built by cutting a cluster from crystal structure.[14, 16, 30]

All PCM calculations were performed with D.01 version of Gaussian 09 package.[31] The absorption maximum has been determined under the non-equilibrium condition, equilibrating the reaction field with respect to the ground-state density, *i.e.*, state-specific non-equilibrium solvation. The vertical emission data is computed with the reaction field consistent with the emitting state, *i.e.*, state-specific equilibrium solvation. The solution-phase analytical $\mathbf{S_0}$ frequencies at DFT level and numerical $\mathbf{S_1}$ frequencies at TD-DFT level have been evaluated to check the absence of imaginary frequencies. The QM/MM was interfaced by using the ChemShell 3.5 package,[32] with the geometry optimized through the hybrid delocalized internal coordinate (HDLC) optimizer.[33] Turbomole 6.5[34-35] and DL-POLY[36] programs were used to calculate the energies and energy gradients of the QM and MM regions, respectively. The electrostatic embedding scheme with QM polarization was adopted.[37] Note that during the QM/MM geometry optimizations, only the QM molecule was active, and the surrounding molecules were kept frozen. The vibrational frequencies were obtained by using a numerical two-point displacement method and the electric polarization of the environment is included.

The structures and energies for the crucial points (*a*, *b*, *c* and *d*) in the adiabatic potential energy surface (PES) were determined at the level of DFT/TD-DFT. No

symmetric constrain was adopted on the geometric optimization for both solution and aggregate. Grimme's D3-correction with Becke-Johnson damping [D3(bj)], was applied to include London-dispersion.[38-40] Optimizations and vibrational-frequency calculations for $\mathbf{S_0}$ and $\mathbf{S_1}$ were performed with PBE0[41] and B3LYP[42-43] functionals using 6-31G* basis set. PBE0 functional has been proved to be one of the most accurate estimates for describing the singlet-excited states of organic molecules from extensive TD-DFT benchmarks.[44-46] In the main text, we will discuss the geometric and energetic properties at the PBE0-D3(bj)/6-31G* level.

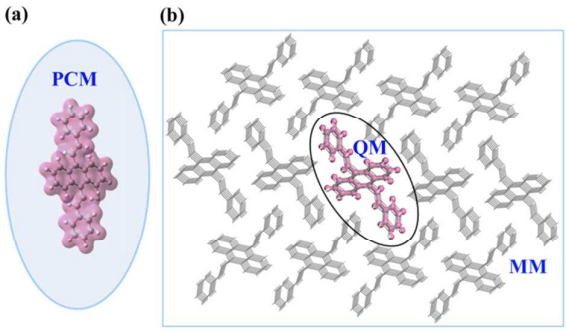

Chart 3. Setup of PCM (a) and QM/MM (b) models (take **DSA** as an example)**.**

3. Results and discussion

3.1 Electronic structure and vertical transition energy

The local minima of $\mathbf{S_0}$ and $\mathbf{S_1}$ are determined by optimizing the geometries and calculating the normal-mode vibrational frequencies. The geometric parameters and energies at *a, b, c* and *d* points in the PES are determined both in solution and in aggregate (see Table S1-S8, ESI†). TD-DFT calculations show that the $\mathbf{S_1}$ states of **DSA**, **DCDPP** and **TPBD** are all dominated by the transition from HOMO to LUMO

in both solution and aggregate phases. The related oscillator strengths and assignments of $\mathbf{S_1}$ are also given (Table S9-S10†). In order to better understand the electronic nature of the excited properties of these molecules, the electronic density contours of HOMOs and LUMOs are plotted (Fig. S4†). The vertical transition energies (E_{ab} and E_{em}), total reorganization energy (λ) and the adiabatic excitation energies (E_{ad}) are obtained according to **Chart 2** (**Table 1** and Table S11-S16†). Vertical transition energies (relevant for absorption and emission peaks) for **DSA**, **DCDPP** and **TPBD** both in solution and aggregate are plotted in **Fig. 1**, together with the experimental values. Detailed comparisons between theoretical calculations at the TD-PBE0-D3(bj)/6-31G* level and the experimental observations are presented in **Table 1**.

Table 1 The electronic vertical transition energies corresponding to absorption and emission peaks for **DSA**, **DCDPP** and **TPBD** in both aggregate and solution phases at the TD-PBE0-D3(bj)/6-31G* level. The available experimental values are presented in the parentheses.

	Absorption			**Emission**		
	E_{ab}^{aggr} /eV	E_{ab}^{solu} /eV	$\Delta E_{ab}^{aggr-solu}$ /eV	E_{em}^{aggr} /eV	E_{em}^{solu} /eV	$\Delta E_{em}^{aggr-solu}$ /eV
DSA	2.96 (2.99[a])	2.79 (3.05[b])	0.17 (-0.06)	2.32 (2.39[c])	2.05 (2.03[b])	0.27 (0.36)
DCDPP	3.49 (3.65[d])	3.34 (3.65[e])	0.15 (0.00)	2.66 (3.00[d])	2.29 (2.93[e])	0.37 (0.07)
TPBD	3.83 (3.60[f])	3.62 (3.71[g])	0.21 (-0.11)	3.09 (3.18[f])	2.58 (3.04[g])	0.51 (0.14)

[a] In THF/water mixture (1:3 by volume), [b]In THF solution (~ 10 μM), [c]Crystal, from Ref. 4.
[d]In THF/water mixture (1:9 by volume), [e]In THF solution (4 μM), from Ref. 5.
[f] In acetone/water mixture (1:9 by volume), [g]In acetone solution (10 μM), from Ref. 6.

Table 2. HOMO and LUMO energies, HOMO-LUMO gaps (eV) at the $\mathbf{S_0}$ equilibrium geometry for **DSA**, **DCDPP** and **TPBD** at the PBE0-D3(bj)/6-31G* and B3LYP-D3(bj)/6-31G* level for aggregate (QM/MM) and solution (PCM)

		Aggregate			Solution		
	Functional	HOMO	LUMO	$\Delta E_{H\text{-}L}$	HOMO	LUMO	$\Delta E_{H\text{-}L}$
	PBE0-D3(bj)	-4.92	-1.41	3.51	-5.28	-1.99	3.29
DSA	B3LYP-D3(bj)	-4.58	-1.37	3.21	-5.01	-2.02	2.99
	PBE0-D3(bj)	-7.23	-3.03	4.20	-6.88	-2.72	4.16
DCDPP	B3LYP-D3(bj)	-6.85	-3.02	3.83	-6.58	-2.78	3.80
	PBE0-D3(bj)	-5.24	-1.00	4.24	-5.61	-1.59	4.02
TPBD	B3LYP-D3(bj)	-4.90	-1.00	3.90	-5.33	-1.64	3.69

It is noticed that for the three compounds: (i) both the predicted absorption maxima (vertical absorption energies) and emission maxima (vertical emission energies) are blue-shifted from solution to aggregate; (ii) the magnitudes of the blue shifts in emission are much more pronounced than those in absorption. Namely, the Stokes shift measuring the difference between the absorption and emission maxima is strongly decreased from solution to aggregate. The former implies that the calculated blue-shifted absorption contributes a portion to the blue-shifted emission according to Equation (2), and could be ascribed to the effect of crystal environment on the frontier molecular orbitals. The calculated HOMO-LUMO energy gaps at their $\mathbf{S_0}$ equilibrium geometry are all larger in aggregate than those in solution for the three molecules (Table 2), indicating that the intramolecular conjugation is diminished upon crystallization. For **DSA**, the dihedral angles between the 9,10-anthraylene core and the vinylene moiety (C27-C31-C32-C28 and C1-C5-C6-C2) of $\mathbf{S_0}$ are about 63° in aggregate, larger than those (53°) in solution. For **DCDPP**, the dihedral angles (C1-C2-C3-C4 and C2-C1-C5-C6) of $\mathbf{S_0}$ are about 45° in aggregate, while the

corresponding values are about 38° in solution. For **TPBD**, two mid-phenyls (C5-C4-C18-C20 and C1-C2-C7-C9) of $\mathbf{S_0}$ are about 69° in aggregate and 64° in solution; two side-phenyls (C4-C5-C40-C42 and C2-C1-C29-C31) of $\mathbf{S_0}$ are approximately 33° in aggregate and 26° in solution. In other words, the twisted peripheral phenyl rings or vinylene moieties help the central planar chromophore struggle to form excimers in aggregate, leading to less effective π conjugation. The latter embodies the important role of the λ term in Equation (2). A large positive term $\lambda^{solu-aggr}$ leads to the remarkable blue-shifted emission found in experiment. It is also possible that blue-shifted emission would occur even when there is no shift or a slight red shift in absorption according to Equation (2). It is noticed that for **DSA**, the calculated blue-shifted value (0.27 eV) is quite similar to that in experiment (0.36 eV), and the experimental solid-phase reference is crystal; while for **DCDPP** and **TPBD**, the available experimental results are for amorphous nanoparticles. It has also been reported that many AIE-active dyes emit blue-shifted lights with higher efficiencies in the crystalline phase than in amorphous phase.[47-49] Our calculations are performed with crystal structure, and therefore for DCDPP and TPBD, the calculated results correlated less well than for DSA. Also, the vertical emission energies are underestimated for **DCDPP** and **TPBD** in solution. To fully address this issue, explicit QM/MM model together with a classic dynamic sampling[50] deserves future investigation. In our QM/MM model for the treatment of aggregates, we completely neglect the excitonic couplings and charge transfer effects, both could account for the slight red-shift in absorption. Indeed, fluorescence of molecular solids is a rather

complicated problem, where both intramolecular (electronic oscillators and vibronic coupling) and intermolecular interactions (exciton diffusion, intermolecular arrangement, long-range order and chemical contamination) [8-9] come to play. In this work, we simply emphasize only one aspect that the blue-shifted emission is induced by intramolecular relaxation, which we believe is essential for such class of molecules.

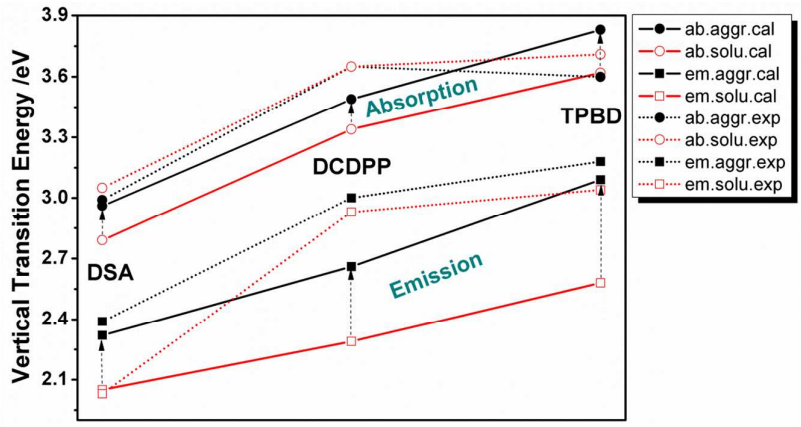

Fig. 1 Vertical transition energies corresponding to both absorption and emission peaks for **DSA**, **DCDPP** and **TPBD** at the PBE0-D3(bj)/6-31G* level. ● and ○ with connected solid [dotted] lines denote the calculated [experimental] vertical absorption energies (ab.) in aggregate (aggr.) and solution (solu.). ■ and □ with connected solid [dotted] lines denote the calculated [experimental] vertical emission energies (em.) in aggregate and solution.

3.2 Rationalization of smaller Stokes shift in aggregate

Stokes' shift is in essence the total reorganization energy during the reciprocal transformation of two electronic states, which can be divided into λ_{gs} and λ_{es}. For clarity, we presented these quantities in **Fig. 2**. It can be seen that the total

reorganization energy are much smaller in aggregate than those in solution. The two components (λ_{gs} and λ_{es}) also follow the same tendency except the counter-intuitive λ_{es} part of **DSA**. This may be ascribed to the "zigzag motif" as shown in **Chart 3**.[14] The peripheral rings nearly perpendicular to the anthracene skeleton have enough space to rotate in aggregate. However, this does not affect the change tendency of the total reorganization energy from solution to aggregate. We turn next to the discussion of geometric relaxation from $\mathbf{S_1}$ to $\mathbf{S_0}$, excited-state configuration and low-frequency out-of-plane vibrations.

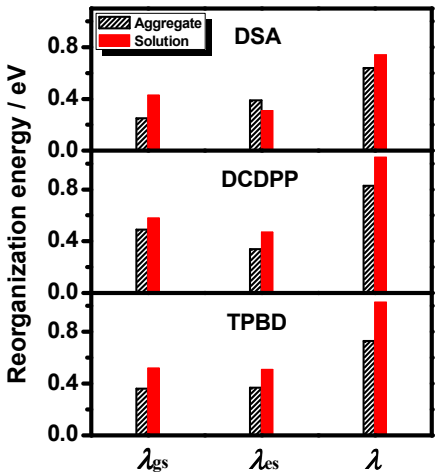

Fig. 2 Total reorganization energy ($\lambda=\lambda_{gs}+\lambda_{es}$) for **DSA**, **DCDPP** and **TPBD** in aggregate and solution at the PBE0-D3(bj)/6-31G* level.

3.2.1 Restricted Geometric modification

The reorganization energy reflects the geometric relaxation in the molecule when going from $\mathbf{S_0}$ to $\mathbf{S_1}$, and *vice versa*. Smaller reorganization energies imply smaller structural changes in aggregate during the excited-state relaxation process. Optimized geometric parameters for these molecules in $\mathbf{S_0}$, $\mathbf{S_1}$ and the structural differences

|Δ(**S$_0$**-**S$_1$**)| are listed, together with X-ray crystal structure for comparison (Table S1-S6 †). The predicted structural parameters of **S$_0$** are in excellent agreement with the crystal structure, which rationalize our QM/MM method. Selected torsion angles with major geometric modifications between **S$_0$** and **S$_1$** are shown in **Fig. 3**. It can be seen that: (i) For **DSA**, a torsion angle between 9,10-anthrylene core and the vinylene moiety (C27-C31-C32-C28) and the central anthracene ring (C31-C4-C1-C5) tends to show a much smaller modification in aggregate from **S$_0$** to **S$_1$**, but the peripheral rings (C32-C28-C38-C45) demonstrate the opposite trend. It is reminiscent of the counter-intuitive λ_{es} part of **DSA.** The electronic density of **DSA** is mainly distributed on the central anthracene ring and the neighboring double bonds and therefore the change in the relatively flexible vinylene moiety together with the central anthracene ring dominates the transition process. (ii) For **DCDPP**, all rotatable rings are restricted in aggregate and show smaller structural differences upon excitation. (iii) For **TPBD**, rotation of the main conjugated butadiene core (C1-C2-C4-C5) together with mid-phenyls (C1-C2-C7-C9) is obviously hindered although two side-phenyls (C2-C1-C29-C31) seem to be slightly active in aggregate. Indeed, the restricted intramolecular motion in aggregate echoes the smaller reorganization energy, and thus causes blue-shifted emission.

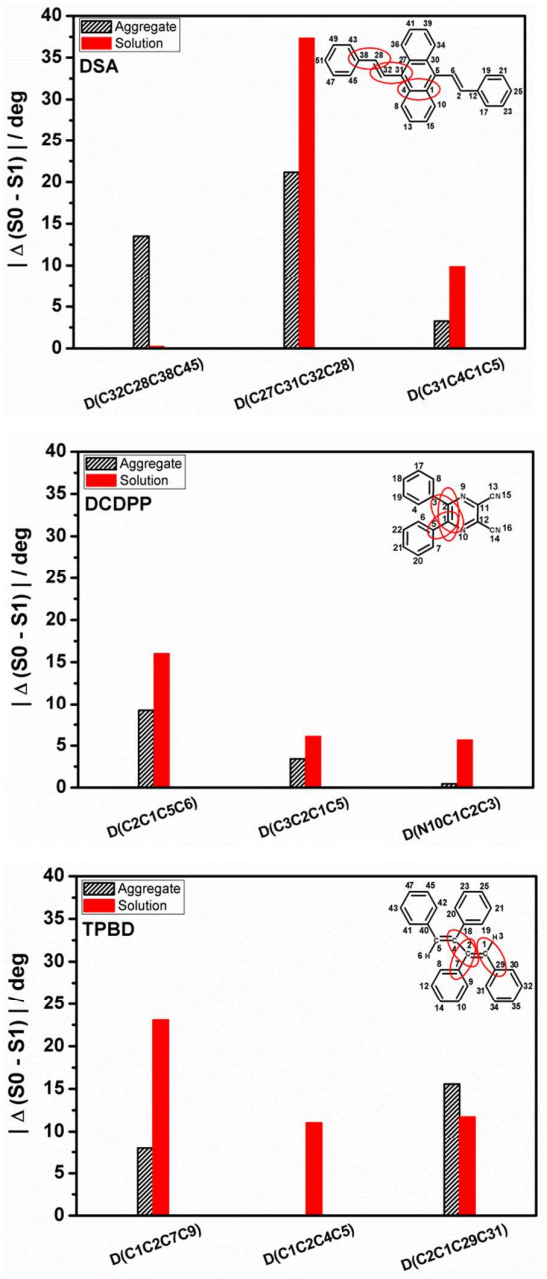

Fig. 3 Selected torsion angles with major geometric modifications between $\mathbf{S_0}$ and $\mathbf{S_1}$ for **DSA**, **DCDPP** and **TPBD** in aggregate and solution at the PBE0-D3(bj)/6-31G* level.

3.2.2 Excited-state planarization

For photoluminescence (PL) spectra in solution, Stokes‘ shift is expected to be smaller if the chromophore shows planar configuration in the excited state.[51] This was

discussed based on broad experimental evidence.[13] Quantum-chemical calculations support such correlation between the excited-state planarization and reduced reorganization energies in solution by studying per-fluoriniation of *para*-oligophenylenes and anilido-pyridine boron difluoride dyes.[52-53] To assess the influence of excited-state planarization, we list the corresponding structural parameters at their $\mathbf{S_0}$ and $\mathbf{S_1}$ equilibrium geometries (see Table S1-S6). It is seen that (i) for **DSA**, the dihedral angles (C31-C4-C1-C5 and C8-C4-C1-C10) related to the central anthracene ring at the $\mathbf{S_1}$ equilibrium geometry are about 5° in aggregate, smaller than those (about 10°) in solution, indicating a relatively planar emitting state formed by anthracene skeleton in aggregate; (ii) for **DCDPP**, the dihedral angles (C11-N9-C2-C3, N10-C1-C2-C3 and C3-C2-C1-C5) of $\mathbf{S_1}$ are about 175°, 175° and 11° in aggregate, respectively. However, the corresponding values are about 169°, 161°, and 21° in solution. This feature also indicates a more planar pyrazine ring in solid phase; (iii) for **TPBD**, the dihedral angle (C1-C2-C4-C5) at the $\mathbf{S_1}$ equilibrium geometry is 180° in aggregate and about 154° in solution, implying a complete planarity of the butadiene core upon aggregation. In other words, excited-state planarization of the central choromophore in aggregate promotes the restricted geometric relaxation, thus leads to the blue-shifted emission.

3.2.3 Freezing of low-frequency out-of-plane vibrations

In the displaced harmonic oscillator model, the Huang-Rhys (HR) factors directly connect with the displacement (D_i) along the normal mode i between the minima of the $\mathbf{S_0}$ and $\mathbf{S_1}$ equilibrium geometries and characterize the extent of

geometric relaxation. The HR factors, $HR_i = \left(\omega_i D_i^2\right)/2\hbar$, are obtained through the DUSHIN program.[54] For **DCDPP**, it has been systematically investigated in our previous work that three modes with large HR factors all fall in the low-frequency region (< 200 cm^{-1}), which are mainly assigned to out-of-plane twisting motions of the phenyl rings.[55] These torsional modes contribute largely to the reorganization energies and result in the large Stokes' shift in gas or solution phase. However, such torsional motions are hindered in aggregate, and the HR factors together with the reorganization energies of the three modes become much smaller, leading to the reduced Stokes shift.[23, 55] For **DSA** and **TPBD**, the large HR factors (HR_i > 1) versus the normal mode at $\mathbf{S_0}$ in both aggregate and solution are listed in **Table 3**. It is seen that (i) there are more vibration modes with large HR factors in solution than in aggregate; (ii) most of these modes display remarkable decrease in HR factors from solution to aggregate, which demonstrates a strong geometric distortion upon excitation in solution; (iii) The diagrammatic illustrations of the selected normal modes in solution with evidently decreased HR factors from solution to aggregate are depicted (Fig. S5†). These coordinates related to the out-of-plane motions are associated with large Stokes shift, much larger than that of other coordinates, such as C-C or C-H stretching. Consequently, these molecules show an emission at significantly longer wavelengths in solution. When these molecules are in a rigid matrix or belong to their crystal, such low-frequency out-of-plane motions are inhibited. Therefore, AIBSE is an obvious consequence of the aggregation-induced

freezing of low-frequency out-of-plane vibrations and of the consequent change of their Franck-Condon factors.

Table 3. Selected normal modes with Huang-Rhys factors (HR_i>1) in aggregate and in solution, as well as harmonic vibrational frequencies (ω_i) of $\mathbf{S_0}$ for **DSA** and **TPBD**.

DSA					
Aggregate			Solution		
mode *i*	ω_i / cm^{-1}	HR_i	mode *i*	ω_i / cm^{-1}	HR_i
3	91	2.07	2	12	3.74
8	158	2.69	3	14	35.98
11	173	6.06	4	25	2.00
17	320	1.74	7	74	3.55
			9	105	10.44
			13	159	1.17
			16	255	1.30
TPBD					
Aggregate			Solution		
mode *i*	ω_i / cm^{-1}	HR_i	mode *i*	ω_i / cm^{-1}	HR_i
8	134	2.21	2	22	12.21
			4	39	5.61
			12	178	1.18

3.3 Robustness of the computational reorganization energy – the effects of ZPE, functionals and basis sets

Now we will discuss the robustness of the computational results. Zero-point vibrational energy (ZPE) correction, choices of functionals, as well as basis-set completeness can certainly affect the computational results. Once considering the

ZPE contribution, both the absorption and emission maxima with respect to the vertical transition energies from the minima of parabola are red-shifted approxiamately 0.03-0.14 eV. Nevertheless, the magnitudes of the red shifts are the same in both absorption and emission, and the ZPE corrected $\Delta E_{\mathrm{em}}^{aggr-solu}$ is still much larger than the ZPE corrected $\Delta E_{\mathrm{ab}}^{aggr-solu}$ for **DSA**, **DCDPP** and **TPBD** (**Table 1** and Table S11†). The reorganization energies keeps unchanged because the ZPE at *a* (*b*) point is the same as that at *d* (*c*) point in the PES (Table S12†). Choices of functionals are now ample. We find that B3LYP-D3(bj) gives nearly the same geometric modification tendency between $\mathbf{S_0}$ and $\mathbf{S_1}$ as PBE0-D3(bj) functional (Table S1-S6†). The vertical transition energies and the reorganization energies of **DSA**, **DCDPP** and **TPBD** are also quite similar to those results at the PBE0-D3(bj)/6-31G* level (Table S13-S15†). TD-DFT generally offers rapid yet accurate estimations for the electronic transition energies.[56-57] The TD-DFT charge-transfer issue is particularly problematic.[58] The recently developed long-range corrected functionals, such as CAM-B3LYP,[59] have shown promise in resolving the charge-transfer deficiencies of TD-DFT.[60] We then recalculated the vertical transition energy and the reorganization energies using CAM-B3LYP-D3(bj) functional based on the structure determined at the (TD)-PBE0-D3(bj)/6-31G* level. The single-point vertical excitation-energy calculations were carried out by adding charges to the QM part with Gaussian 09 program. The added charges mimic the surrounding MM parts obtained by the above QM/MM optimizations. The vertical transition energies for the three molecules with the long-range corrected

CAM-B3LYP-D3(bj) functional are blue-shifted about 0.13-0.54 eV in comparison with those obtained by using PBE0-D3(bj) functional, also in agreement with experimental results (Table S17†). And most importantly, the pronounced positive $\lambda^{solu\text{-}aggr}$ nature is kept unchanged (Table S18†).

Basis-set incompleteness errors (BSIE) were noticed and should be benchmarked. To reduce the computational efforts, single-point vertical excitation-energy calculations were carried out based on the stable structures determined at the (TD)-PBE0-D3(bj)/6-31G* level. We have evaluated the dependence of larger TZVP with triple-ζ quality and 6-31+G* with a diffuse function on the vertical transition energies and reorganization energies. It was found that when going from double-ζ 6-31G* to triple-ζ TZVP, the vertical transition energies were decreased by about 0.02-0.09 eV (Table S19†). Addition of diffuse functions to second-row elements in the periodic table gives the same magnitudes of red shifts (Table S20†). Even so, the values of $\lambda^{solu\text{-}aggr}$ terms are almost the same as the small 6-31G* basis set (Table S21-S22†).

Thus, through extensive computations, we find the effects of ZPE, functionals and basis sets do not change the quantitative conclusions.

4. Conclusion

To summarize, we have presented a multiscale quantum chemistry investigation on the exotic AIBSE phenomenon, *i.e.*, the absorption is relatively unaffected but the emission undergoes a remarkable blue shift from solution to aggregate, taking **DSA**,

DCDPP and **TPBD** as examples, in sharp contrast to the conventional solid-state red-shifted emitting behavior. We point out this is primarily originated from the smaller reorganization energy in aggregate compared to the solution, as induced by restricted geometric change, excited-state planarization and freezing of low-frequency out-of-plane vibrations during the excited-state relaxation. Through computational chemistry, we justify this assumption by determining the structures and energies for the crucial points (*a*, *b*, *c* and *d*) in the PES taking both solvent effect and aggregation environment into account, using PCM and QM/MM approaches, respectively. The theoretical results render supports to the existing experimental findings and reveal the nature of the AIBSE phenomena. In fact, from this study, we conclude that such blue shift is universal if the AIE mechanism is indeed the restricted intramolecular rotation (RIR). Namely, aggregation tends to suppress the non-radiative decay process through intermolecular hindrance, while leaving radiative decay dominant. The AIBSE is another outcome of such effect.

In the present method, the following approximations are made: (i) we assumed that the intermolecular interactions are weak and there are no appreciable intermolecular charge or energy transfers or excitonic effect between neighboring molecules; (ii) MM polarization by the electron-density change of the QM molecule in the excited state was not taken into account due to the limitation of GAFF. Conventional molecular exciton theory usually takes one or two vibrational modes with fixed exciton-vibration coupling (Huang-Rhys factor). Nevertheless, in this work, we shine light on the molecular picture mentioned above, induced by restricted

intramolecular motion in aggregate, leads to the blue-shifted emission. So far, excitonic model often ignored the molecular feature. This work cautions the application of such treatment.

Acknowledgement

TZ is deeply indebted to Dr. Likai Du for the help about the QM/MM method and Dr. Peng Cui concerning the computational codes. The authors thank Profs. Junwu Chen and Wenjing Tian, and Dr. Bin Xu for extensive discussions on their experimental findings. This work is supported the National Natural Science Foundation of China (Grant Nos. 21290190, 21103097, 21121004, and 91233105), and the Ministry of Science and Technology of China through 973 program (Grant Nos. 2013CB834703, 2013CB933503, and 2011CB808400).

1 J. A. Rogers, T. Someya and Y. G. Huang, *Science*, 2010, **327**, 1543-1678.
2 R. D. Miller and E. A. Chandross, *Chem. Rev.*, 2010, **110**, 1-574.
3 W. Z. Yuan, P. Lu, S. M. Chen, J. W. Y. Lam, Z. M. Wang, Y. Liu, H. S. Kwok, Y. G. Ma and B. Z. Tang, *Adv. Mater.*, 2010, **22**, 2159-2163.
4 W. Z. Yuan, Y. Q. Tan, Y. Y. Gong, P. Lu, J. W. Y. Lam, X. Y. Shen, C. F. Feng, H. H. Y. Sung, Y. W. Lu, I. D. Williams, J. Z. Sun, Y. M. Zhang and B. Z. Tang, *Adv. Mater.*, 2013, **25**, 2837-2843.
5 J. Gierschner, L. Lüer, B. Milián-Medina, D. Oelkrug and H.-J. Egelhaaf, *J. Phys. Chem. Lett.*, 2013, **4**, 2686-2697.
6 Y. N. Hong, J. W. Y. Lam and B. Z. Tang, *Chem. Commun.*, 2009, 4332-4353.
7 Y. N. Hong, J. W. Y. Lam and B. Z. Tang, *Chem. Soc. Rev.*, 2011, **40**, 5361-5388.
8 J. Gierschner and S. Y. Park, *J. Mater. Chem. C*, 2013, **1**, 5818-5832.
9 D. Oelkrug, A. Tompert, H.-J. Egelhaaf, M. Hanack, E. Steinhuber, M. Hohloch, H. Meier and U. Stalmach, *Synth. Met.*, 1996, **83**, 231-237.
10 Y.-S. Huang, J. Gierschner, J. P. Schmidtke, R. H. Friend and D. Beljonne, *Phys. Rev. B*, 2011, **84**, 205311.

11 B.-K. An, S.-K. Kwon, S.-D. Jung and S. Y. Park, *J. Am. Chem. Soc.*, 2002, **124**, 14410-14415.
12 Y. J. Dong, B. Xu, J. B. Zhang, X. Tan, L. J. Wang, J. L. Chen, H. G. Lv, S. P. Wen, B. Li, L. Ye, B. Zou and W. J. Tian, *Angew. Chem. Int. Ed.*, 2012, **51**, 10782-10785.
13 D. Oelkrug, A. Tompert, J. Gierschner, H.-J. Egelhaaf, M. Hanack, M. Hohloch and E. Steinhuber, *J. Phys. Chem. B*, 1998, **102**, 1902-1907.
14 J. T. He, B. Xu, F. P. Chen, H. J. Xia, K. P. Li, L. Ye and W. J. Tian, *J. Phys. Chem. C*, 2009, **113**, 9892-9899.
15 Y. J. Dong, B. Xu, J. B. Zhang, H. G. Lu, S. P. Wen, F. P. Chen, J. T. He, B. Li, L. Ye and W. J. Tian, *CrystEngComm*, 2012, **14**, 6593-6598.
16 A. J. Qin, J. W. Y. Lam, F. Mahtab, C. K. W. Jim, L. Tang, J. Z. Sun, H. H. Y. Sung, I. D. Williams and B. Z. Tang, *Appl. Phys. Lett.*, 2009, **94**, 253308.
17 J. W. Chen, B. Xu, X. Y. Ouyang, B. Z. Tang and Y. Cao, *J. Phys. Chem. A*, 2004, **108**, 7522-7526.
18 Z. Li, Y. Q. Dong, B. X. Mi, Y. H. Tang, M. Häussler, H. Tong, Y. P. Dong, J. W. Y. Lam, Y. Ren, H. H. Y. Sung, K. S. Wong, P. Gao, I. D. Williams, H. S. Kwok and B. Z. Tang, *J. Phys. Chem. B*, 2005, **109**, 10061-10066.
19 K. A. N. Upamali, L. A. Estrada, P. K. De, X. C. Cai, J. A. Krause and D. C. Neckers, *Langmuir*, 2011, **27**, 1573-1580.
20 X. Y. Shen, Y. J. Wang, E. G. Zhao, W. Z. Yuan, Y. Liu, P. Lu, A. J. Qin, Y. G. Ma, J. Z. Sun and B. Z. Tang, *J. Phys. Chem. C*, 2013, **117**, 7334-7347.
21 R. R. Hu, E. Lager, A. l. Aguilar-Aguilar, J. Z. Liu, J. W. Y. Lam, H. H. Y. Sung, I. D. Williams, Y. C. Zhong, K. S. Wong, E. Peña-Cabrera and B. Z. Tang, *J. Phys. Chem. C*, 2009, **113**, 15845-15853.
22 M.-C. Li, M. Hayashi and S.-H. Lin, *J. Phys. Chem. A*, 2011, **115**, 14531-14538.
23 Q. Y. Wu, C. M. Deng, Q. Peng, Y. L. Niu and Z. G. Shuai, *J. Comput. Chem.*, 2012, **33**, 1862-1869.
24 Q. Y. Wu, Q. Peng, Y. L. Niu, X. Gao and Z. G. Shuai, *J. Phys. Chem. A*, 2012, **116**, 3881-3888.
25 M. Cossi and V. Barone, *J. Chem. Phys.*, 2001, **115**, 4708-4717.
26 G. Scalmani, M. J. Frisch, B. Mennucci, J. Tomasi, R. Cammi and V. Barone, *J. Chem. Phys.*, 2006, **124**, 094107.
27 R. Improta, V. Barone, G. Scalmani and M. J. Frisch, *J. Chem. Phys.*, 2006, **125**, 054103.
28 A. Warshel and M. Levitt, *J. Mol. Biol.*, 1976, **103**, 227-249.
29 J. M. Wang, R. M. Wolf, J. W. Caldwell, P. A. Kollman and D. A. Case, *J. Comput. Chem.*, 2004, **25**, 1157-1174.
30 I. L. Karle and K. S. Dragonette, *Acta Cryst.*, 1965, **19**, 500-503.
31 M. J. Frisch, G. W. Trucks, H. B. Schlegel, G. E. Scuseria, M. A. Robb, J. R. Cheeseman, G. Scalmani, V. Barone, B. Mennucci, G. A. Petersson, H. Nakatsuji, M. Caricato, X. Li, H. P. Hratchian, A. F. Izmaylov, J. Bloino, G. Zheng, J. L. Sonnenberg, M. Hada, M. Ehara, K. Toyota, R. Fukuda, J. Hasegawa, M. Ishida, T. Nakajima, Y. Honda, O. Kitao, H. Nakai, T. Vreven, J. A. Montgomery, Jr., J. E.

Peralta, F. Ogliaro, M. Bearpark, J. J. Heyd, E. Brothers, K. N. Kudin, V. N. Staroverov, R. Kobayashi, J. Normand, K. Raghavachari, A. Rendell, J. C. Burant, S. S. Iyengar, J. Tomasi, M. Cossi, N. Rega, J. M. Millam, M. Klene, J. E. Knox, J. B. Cross, V. Bakken, C. Adamo, J. Jaramillo, R. Gomperts, R. E. Stratmann, O. Yazyev, A. J. Austin, R. Cammi, C. Pomelli, J. W. Ochterski, R. L. Martin, K. Morokuma, V. G. Zakrzewski, G. A. Voth, P. Salvador, J. J. Dannenberg, S. Dapprich, A. D. Daniels, Ö. Farkas, J. B. Foresman, J. V. Ortiz, J. Cioslowski, and D. J. Fox, Gaussian 09, Revision D.01, GaussianInc., Wallingford CT, 2013.

32 P. Sherwood, A. H. de Vries, M. F. Guest, G. Schreckenbach, C. R. A. Catlow, S. A. French, A. A. Sokol, S. T. Bromley, W. Thiel, A. J. Turner, S. Billeter, F. Terstegen, S. Thiel, J. Kendrick, S. C. Rogers, J. Casci, M. Watson, F. King, E. Karlsen, M. Sjøvoll, A. Fahmi, A. Schäfer and C. Lennartz, *J. Mol. Struct. : Theochem*, 2003, **632**, 1-28.

33 S. R. Billeter, A. J. Turner and W. Thiel, *Phys. Chem. Chem. Phys.*, 2000, **2**, 2177-2186.

34 TURBOMOLE V6.5 2013, University of Karlsruhe and of the Forschungszentrum Karlsruhe GmbH, 1989-2007; TURBOMOLE GmbH, since 2007 (accessed May 23, 2013).35 R. Ahlrichs, M. Bär, M. Häser, H. Horn and C. Kölmel, *Chem. Phys. Lett.*, 1989, **162**, 165-169.

36 W. Smith and T. R. Forester, *J. Mol. Graphics*, 1996, **14**, 136-141.

37 D. Bakowies and W. Thiel, *J. Phys. Chem.*, 1996, **100**, 10580-10594.

38 S. Grimme, J. Antony, S. Ehrlich and H. Krieg, *J. Chem. Phys.*, 2010, **132**, 154104.

39 S. Grimme, S. Ehrlich and L. Goerigk, *J. Comput. Chem.*, 2011, **32**, 1456-1465.

40 L. Goerigk and J. R. Reimers, *J. Chem. Theory Comput.*, 2013, **9**, 3240-3251.

41 C. Adamo and V. Barone, *J. Chem. Phys.*, 1999, **110**, 6158-6170.

42 A. D. Becke, *J. Chem. Phys.*, 1993, **98**, 5648-5652.

43 C. Lee, W. T. Yang and R. G. Parr, *Phys. Rev. B*, 1988, **37**, 785-789.

44 D. Jacquemin, E. A. Perpète, I. Ciofini and C. Adamo, *Acc. Chem. Res.*, 2009, **42**, 326-334.

45 D. Jacquemin, V. Wathelet, E. A. Perpète and C. Adamo, *J. Chem. Theory Comput.*, 2009, **5**, 2420-2435.

46 D. Jacquemin, A. Planchat, C. Adamo and B. Mennucci, *J. Chem. Theory Comput.*, 2012, **8**, 2359-2372.

47 J. W. Chen, B. Xu, K. X. Yang, Y. Cao, H. H. Y. Sung, I. D. Williams and B. Z. Tang, *J. Phys. Chem. B*, 2005, **109**, 17086-17093.

48 Y. Q. Dong, J. W. Y. Lam, A. J. Qin, Z. Li, J. Z. Sun, H. H. Y. Sung, I. D. Williams and B. Z. Tang, *Chem. Commun.*, 2007, 40-42.

49 H. Tong, Y. Dong, Y. Hong, M. Häussler, J. W. Y. Lam, H. H. Y. Sung, X. Yu, J. Sun, I. D. Williams, H. S. Kwok and B. Z. Tang, *J. Phys. Chem. C*, 2007, **111**, 2287-2294.

50 N. De Mitri, S. Monti, G. Prampolini and V. Barone, *J. Chem. Theory Comput.*, 2013, **9**, 4507-4516.

51 I. B. Berlman, *J. Phys. Chem.*, 1970, **74**, 3085-3093.

52 B. Milián-Medina, S. Varghese, R. Ragni, H. Boerner, E. Ortí, G. M. Farinola and J. Gierschner, *J. Chem. Phys.*, 2011, **135**, 124509.
53 J.-L. Jin, H.-B. Li, Y. Geng, Y. Wu, Y.-A. Duan and Z.-M. Su, *ChemPhysChem*, 2012, **13**, 3714-3722.
54 J. R. Reimers, *J. Chem. Phys.*, 2001, **115**, 9103-9109.
55 C. M. Deng, Y. L. Niu, Q. Peng, A. J. Qin, Z. G. Shuai and B. Z. Tang, *J. Chem. Phys.*, 2011, **135**, 014304.
56 D. Jacquemin, E. A. Perpète, G. Scalmani, M. J. Frisch, I. Ciofini and C. Adamo, *Chem. Phys. Lett.*, 2007, **448**, 3-6.
57 D. Jacquemin, E. A. Perpète, G. Scalmani, I. Ciofini, C. Peltier and C. Adamo, *Chem. Phys.*, 2010, **372**, 61-66.
58 A. Lange and J. M. Herbert, *J. Chem. Theory Comput.*, 2007, **3**, 1680-1690.
59 T. Yanai, D. P. Tew and N. C. Handy, *Chem. Phys. Lett.*, 2004, **393**, 51-57.
60 M. A. Rohrdanz, K. M. Martins and J. M. Herbert, *J. Chem. Phys.*, 2009, **130**, 054112.

ToC

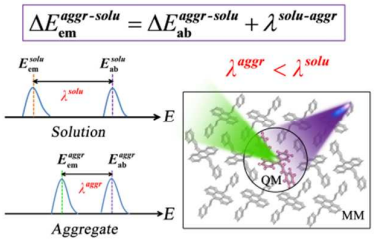

Aggregation induced blue-shifted emission is a consequence of the restricted structural relaxation, excited-state planarization and freezing of low-frequency out-of-plane vibrations vibrations.